Chapter 6
Comparison of Protein Interaction with Different Shaped PbS Nanoparticles and Corona Formation

A. K. Mishra, A. K. Bhunia, and S. Saha

Abstract Different shaped PbS nanoparticles are synthesized at room temperature by using reagents, lead chloride ($PbCl_2$), sulfur powder (S), and sodium borohydride ($NaBH_4$), in the ethylenediamine medium. $NaBH_4$ has acted as a reducing agent, whereas ethylenediamine is used as a capping agent. The grown PbS nanoparticles are spherical (7 nm size) for the reagent ratio of $PbCl_2$, S, $NaBH_4$ as 1:1:1. and grown PbS nanoparticles are cubical shape (13 nm size) for the reagent ratio of $PbCl_2$, S, $NaBH_4$ as 1:1:3. The grown PbS nanoparticles are characterized structurally and optically. The interaction and formation of the bio-conjugate of bovine serum albumin with PbS nanomaterials are studied for biomedical application. The interaction, complexion process, and conformational changes of bovine serum albumin with PbS nanomaterials are quantified by the photophysical and structural study. PbS nanomaterials enable the aggregation of bovine serum albumin by the way of unfolding. The interaction and the bioconjugate formation of albumin with PbS nanoparticles are investigated using optical spectroscopy, TEM. UV–VIS–NIR shows the binding process that occurred between albumin and PbS samples.

6.1 Introduction

Now the recent trend of using nanotechnology increases more and more in the field of agriculture, biomedicine, packaging, cosmetics, and also in textiles. There are possibilities that these nanoparticles (NPs) are entering living organ cells through various natural processes like the food chain, respiration, etc. NPs are not used for biological imaging due to optical emission in the infrared region as many proteins strongly absorb visible light, so there is a limitation in the depth of penetration around few millimeters in the small wavelengths region. Another biological complex like

A. K. Mishra (✉) · S. Saha
Department of Physics, Vidyasagar University, Paschim Medinipur, Midnapore, West Bengal 721102, India

A. K. Bhunia
Department of Physics , Government General Degree College at Gopiballavpur-II , Jhargram, Beliaberah, West Bengal 721517, India

S. Sengupta et al. (eds.), *Selected Progresses in Modern Physics*, Springer Proceedings in Physics 265, https://doi.org/10.1007/978-981-16-5141-0_6

water and lipids strongly absorbs infrared light [1, 2]. PbS semiconducting NPs are an important IV–VI group due to their near-infrared (NIR) fluorescence property for bio-imaging applications. PbS semiconducting quantum dots with diameters between 3 and 6 nm show an emission wavelength in the NIR region. So PbS NPs have been projected as one of the best potential materials for application in various biomedical detection of animal studies [3]. Only 10–15 proteins may take part in protein corona formation from thousands of proteins in physiological conditions [4–8], that is, the exchange of soft corona proteins by hard corona proteins [9–11]. This hard protein corona helps the NPs in intracellular signaling due to longer life and also identifies the role of NPs in biological fluid [12]. This nano–bio interaction of different shaped PbS NPs is important in nanomedicine research due to physicochemical properties. The PbS NPs surface area surrounded by an assembly of proteins is known as protein corona and their complex is called the protein–PbS NPs complex. The protein corona formation process is playing a vital role in the functioning of PbS NPs in the biological system. The native structure of protein shows conformational change due to the interaction of PbS NPs with protein. This vibrant and driving process changes the functioning of protein for cellular interaction with PbS NPs [13, 14]. Yin et al. [15] evaluated the cytotoxic behavior of bared and protein-coated ZnO NPs against human hepatocellular carcinoma (HepG2) cells and they found that bare ZnO NPs at a concentration range of 20 mg L^{-1}–100 mg L^{-1} reduced the cell viability by 90–15%, whereas for protein-coated ZnO NPs, cell viability was reduced by only 5–15% even at 100 mg L^{-1} concentration. They proposed that the higher binding strength between protein and NPs prevented the generation of reactive oxygen species (ROS) due to which protein-coated ZnO NPs showed less cytotoxicity. Medina et al. [16] evaluated the role of protein concentration (BSA) on the NPs toxicity, protein adsorption, and NPs accumulation. They compared the intracellular uptake of gold nanorods coated with a cationic agent mercaptoundecyltrimethylammonium bromide (MUTAB-AuNRs) in MCF-7 cancer cells. They incubated the MUTAB-AuNRs directly in 10% fetal bovine serum (FBS) and compared it with MUTAB-AuNRs preincubated (1% BSA) with a low concentration of BSA (1%) and reported that preincubation in 1% BSA increased the intracellular uptake by three times. It could be due to the lower concentration of BSA (in comparison to physiological conditions), which has increased the entry of AuNRs into MCF-7 cancer cells. Luminescence correlation spectroscopy and UV–visible spectroscopy analysis suggested that the concentration of preincubation played an important role in the correlation decay and the agglomeration of NPs. Hence, diagnostics tests based on this corona analysis will become more efficient than the ordinary running biochemical test. So different techniques can be applied for the analysis of protein corona to get information on molecular consequence due to contact of PbS NPs. C. Vidaurre-Agut et al. [17] found that diagnostic tests which performed depending on proteomics analysis have more advantage than traditional biochemical tests. It is difficult to identify protein biomarkers which have a low molecular weight (MW) by standard mass spectrometer because these are normally at low concentrations and are masked by actual abundant resident proteins. They showed that mesoporous silica NPs were able to capture low MW protein comparatively better than the protein

corona (PC) adsorbed onto dense silica NPs from serum. They further investigated this effect using liquid chromatography − mass spectrometry (LC–MS) and thermogravimetric analysis (TGA) and compared the MW of the proteins in the coronas of mesoporous silica NPs with the same particle size but different pore diameters. They also examined the process by which two proteins, one small and one large, adsorb onto these mesoporous silica NPs to establish a theory of why the corona became enriched in low MW proteins. They developed a novel system for the diagnosis of prostate cancer and this was applied to LC − MS protein coronas from the serum of 22 cancer patients, identifying proteins specific to each patient group. They explained why low MW proteins predominate in the coronas of mesoporous silica NPs, and they illustrated the ability of this information to supplement more traditional diagnostic tests.

Experimental observation is carried out to understand the protein–PbS NPs complex for well-suited NPs with surface characterization for better biological application. The interaction of PbS NPs with bovine serum albumin (BSA) is studied and the bio-safety of exposed PbS NPs is determined. The "hard" and "soft" protein PbS NPs corona formation is represented by the interaction of PbS NPs with protein.

6.2 Experimental Section

The PbS NPs were synthesized by anhydrous lead chloride ($PbCl_2$) (99.999%), sulfur powder (99.999%), and an amount of sodium borohydride ($NaBH_4$) (99%). The ratio of a reagent was calculated assuming that all of the reagents are consumed but there is no excess of reagents in reaction completion. The ratio was calculated by the amount of mass multiplied by the molar mass of each reactant to the no of molecules required for each reactant per mole of reaction. In this method, $NaBH_4$ is used as a reducing agent to initiate the reaction between $PbCl_2$ and S at room temperature (25 C). Ethylenediamine (EDA) was used as a solvent. At first, an amount of 2.78 g $PbCl_2$ was dissolved in 50 ml of EDA. This solution was taken in a beaker and was stirred vigorously by using a magnetic stirrer. After 30 min, 0.32 g of sulfur was added to the above solution. Finally, 0.37 g and 1.11 g of $NaBH_4$ were added to two beakers, respectively, by taking the same amount of the above mixture to get grown PbS samples of different ratios. The solution was stirred for 4 h keeping the particular speed for all samples. The solution was turned into a black color. This was an indication of the formation of PbS NPs. The residue product of grown samples was washed with distilled water several times. Finally, the product samples were centrifuged and were kept for 2 weeks in a clean dry place at room temperature. The chemical reaction for PbS NPs preparation is given below

$$PbCl_2 = Pb^{+2} + 2Cl^-$$

$$NaBH_4 + 2Cl^- = NaCl + B_2H_6 + 2H + 2e^-$$

$$2H + S = H_2S$$

$$H_2S + Pb^{+2} + 2e^- = PbS + H_2$$

The grown PbS NPs were dispersed in deionized water by ultrasonication for 30 min. The PbS NPs concentration was varied from 0.01 mg/mL to 0.06 mg/mL. Now for the PbS–BSA-mixed solutions preparation, 0.1 mg/mL BSA is mixed with PbS NPs ranging from 0.01 to 0.06 mg/mL with proper ratio.

High-resolution Rigaku Mini Flex X-ray Diffractometer was used to get the X-ray diffraction (XRD) pattern of powder PbS nanosamples. Transmission electron microscopy (TEM) was done by JEOL-JEM-2100. The carbon-coated copper grid was taken and a solution sample of PbS NPs was dropped on it after properly disperse in distilled water medium and dried in the dust-free region. Scanning electron microscopy (SEM) image of powder PbS nanosamples obtained by JEOL-JSM 5800. Agilent Technologies Cary 5000 Series UV–VIS–NIR Spectrophotometer is used to obtain Optical absorption spectra of PbS nanosamples and conjugate solution with BSA immediately after ultrasonication concerning deionized water.

6.3 Result and Discussion

6.3.1 Absorption Study

The absorption spectra of tryptophan (TRY) of BSA with different concentrations of the different shaped PbS NPs and pure PbS NPs.

The absorption peak for TRY of BSA is seen at 280 nm in Fig. 6.1. This transition may correspond to π–π* transition of aromatic amino acid residues [18, 19].

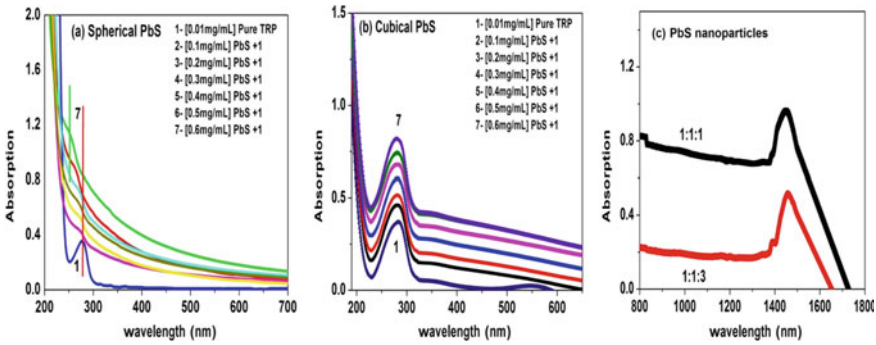

Fig. 6.1 Shows the absorption spectra of (a) tryptophan (TRY) of BSA with spherical PbS, (b) tryptophan (TRY) of BSA with cubical PbS, and (c) pure PbS NPs

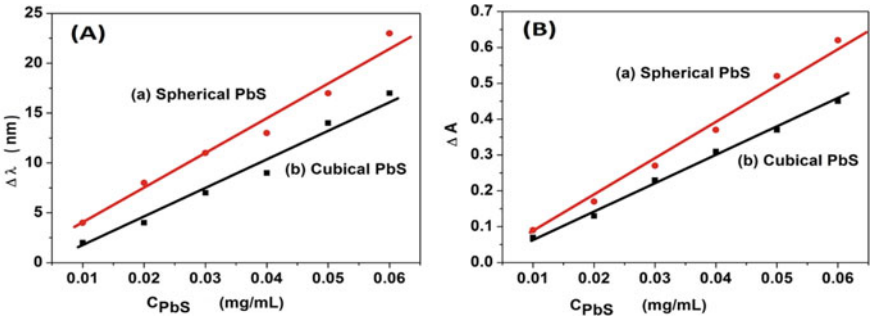

Fig. 6.2 Shows the plots of (A) C_{PbS} vs change in wavelength ($\Delta\lambda$) and (B) C_{PbS} vs change in absorbance (ΔA) for different shaped PbS NPs

The effect of binding of PbS NPs with concentrations ($C_{PbS} = 0.01$–0.06 mg/ml) with BSA ($C_{BSA} = 0.1$ mg/mL) is shown in Fig. 6.2.

These results show that the absorbance of TRY of BSA increases with the increment of C_{PbS} in Fig. 6.1. This intensity of absorbance of BSA gradually increases with C_{PbS}, due to the binding of BSA with PbS NPs and the formation of the ground state complex [20]. The absorption band of BSA is red-shifted gradually with an increment of C_{PbS}. This also confirms that PbS NPs interact with BSA through TRY and induces the conformational change of BSA [21]. The plots of C_{PbS} vs change in wavelength ($\Delta\lambda$) and C_{PbS} vs change in absorbance (ΔA) is shown in Fig. 6.2.

The plots of C_{PbS} vs change in wavelength ($\Delta\lambda$) are linear fit and C_{PbS} vs change in absorbance (ΔA) is shown that the interaction of BSA with PbS NPs increases with the increase of C_{PbS}.

In the equilibrium condition, the complex formation between PbS NPs and protein is given by the equation, where K_{app} is the apparent association constant.

$$K_{app}$$

$$\text{Tryptophan (Protein)} + \text{PbS nanoparticles} = \text{Protein.....PbS nanoparticles}$$

$$\text{Kapp} = \frac{[\text{Protein.....PbS nanoparticles}]}{[\text{Protein}][\text{PbS nanoparticles}]}$$

These K_{app} values are obtained using Benassi and Hildebrand method [19] and the equation is also given as

$$J_{obs} = (1 - \alpha)\, A_0 + \alpha\, A_c$$

Where A_{obs} is the value of absorbance of TRY (Protein) solution with different concentrations of PbS NPs and α is the degree of association between TRY (Protein)

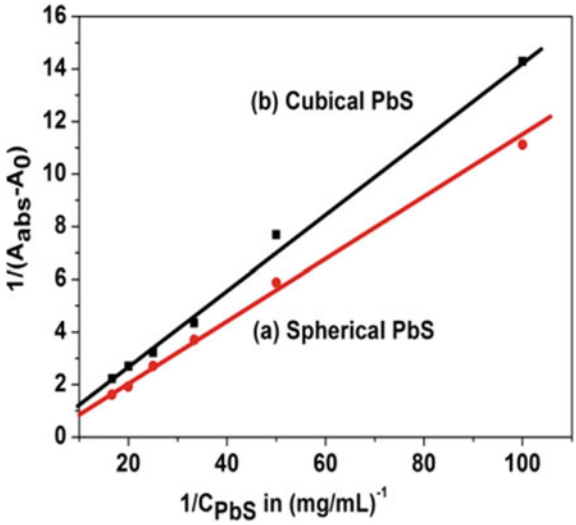

Fig. 6.3 Shows the plot of $\frac{1}{\text{Aobs}-\text{A0}}$ versus $1/C_{PbS}$ for different shaped PbS NPs

solution with PbS NPs. Here, A_0 and A_c are the absorbances of TRY (Protein) and complex of Protein and PbS NPs. This equation also can be written as

$$\frac{1}{\text{Aobs} - \text{A0}} = \frac{1}{\text{Ac} - \text{A0}} + \frac{1}{(\text{Ac} - \text{A0})\text{Kapp}[\text{CPbS}]}$$

Therefore, the plot of $\frac{1}{\text{Aobs}-\text{A0}}$ versus $1/C_{PbS}$ is linear fit with the slope $\frac{1}{(\text{Ac}-\text{A0})\text{Kapp}}$ and intercept to the axis is $\frac{1}{\text{Ac}-\text{A0}}$. From these data, K_{app} is also calculated.

The plot of $\frac{1}{\text{Aobs}-\text{A0}}$ versus $1/C_{PbS}$ for different shaped PbS NPs are shown in Fig. 6.3.

The absorption spectra show peaks at NIR and UV region for PbS NPs and BSA solution, respectively. The photoluminescence spectra of different shaped PbS NPs show emission in the NIR region. whereas the UV region for BSA protein [15].

PbS NPs come in contact with BSA and are surrounded by protein molecules. PbS NPs form a dynamic layer of proteins on the surface after getting associated with the BSA. Hence, *"NPs − protein corona"* is formed by this conjugated system[13, 22]. The change in absorbance intensity (ΔA) of BSA with $C_{BSA} = 0.1$ mg/mL is shown in Fig. 6.2(B) to detect the corona formation, and conformational changes of BSA are seen in the presence of PbS NPs. The change in absorbance intensity of BSA increases with PbS NP concentrations as well as decreases with the increase of PbS NP size.

It is confirmed from the exponential association mechanism that the "PbS NPs-BSA" corona formation starts just after incorporation of PbS NPs into BSA, whereas it is continued for a very long time to unfold the BSA. Hence, the BSA takes a long time to shield the PbS NPs surface with confirmation change and the BSA is unfolded [23–25]. The hard corona [22] is formed. The change of absorption intensity of BSA

(ΔA) in interaction with PbS NPs ($C_{PbS} = 0.1$ mg/mL to 0.6 mg/mL (Fig. 6.2(B)) shows a linear fit. The PbS NPs–BSA corona is formed at an inner layer of unfolded BSA using a slow exchange rate with free BSA (hard corona) whereas an outer layer of weakly bound BSA which follows linear kinetics and regarded as a faster exchange rate with free BSA (soft corona) [26–29].

6.3.2 XRD Study

The XRD pattern of the different shaped PbS NPs is shown in Fig. 6.4.

The X-Ray diffraction pattern is used to study the structural phase of the grown PbS NPs. The X-ray diffraction is taken with an angular range (2θ) from 20 to 80 degrees. The prominent diffraction peaks are (111), (2 00), (22 0), (311), (222), (400), (331), (420) correspond to pure face-centered cubic (FCC) phase (JCPDS # 05–0592) of the unit cell of PbS NPs. These planes are well matched with the standard crystal planes (111), (2 00), (22 0), (311), (222), (400), (331), (420) for diffraction angle 20–80° according to JCPDS no. 05–0592 [30, 31]. The highest intensity and sharp peak prove the well crystalline nature of grown PbS NPs. The size of PbS samples obtained from the Debye–Scherrer equation [31], D = 0.9 **λ** /(β COSθ), where D is particle size in nm**,** **λ** is the X-ray wavelength in nm, θ *is*, the diffraction angle in degrees, and β is the maximum peak width in half-height. The grown spherical PbS NPs are 7 nm in size and grown cubical shape PbS NPs are 13 nm in size.

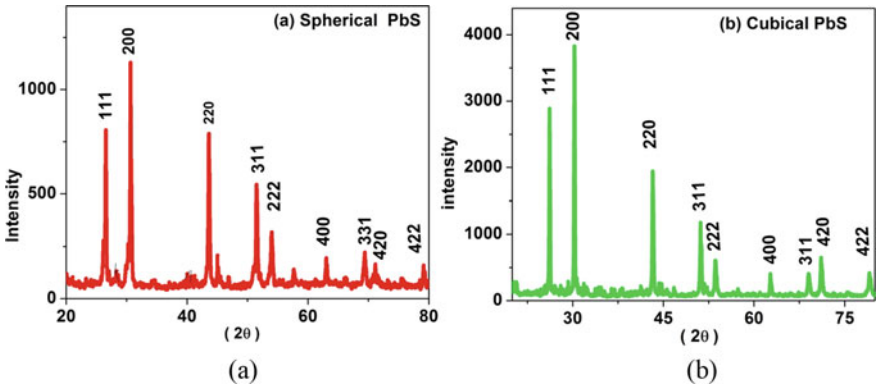

Fig. 6.4 Shows the XRD pictures of (a) spherical-shaped PbS NPs, (b) cubical PbS NPs

6.3.3 TEM Study

TEM pictures of spherical-shaped PbS NPs, corona formation with BSA, and SAED pattern are shown in Fig. 6.5.

There are shown in the figure the hard and soft corona structures formed by spherical-shaped PbS NPs under experimental conditions. The hard corona is represented by the inner blackish core. The *soft corona*" formation is represented by the outer fractal layer of BSA which is loosely bound with "*hard corona*". The hard coronas that almost spherical PbS NPs with a diameter of 260 nm are strongly attached to BSA. The image of a hard corona is shown by the arrow mark. This image represents that the core PbS NPs are fully covered with BSA along with a shell thickness of 7.5 nm which is matched with a dimension of BSA with 8 nm, calculated from protein data bank [6].

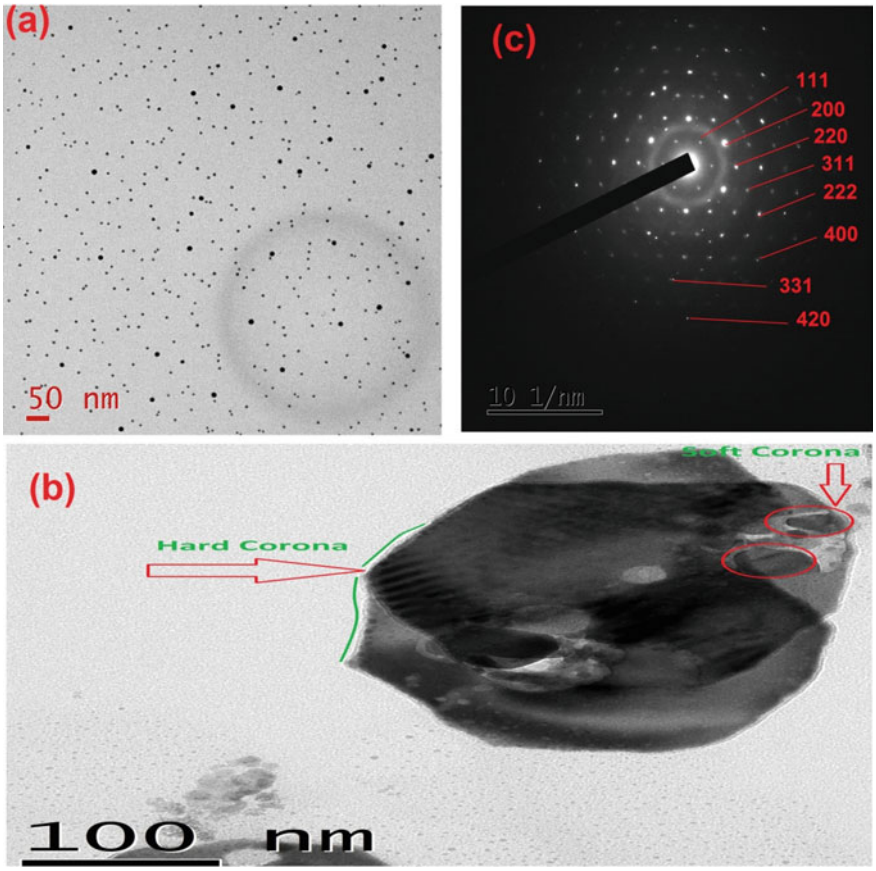

Fig. 6.5 Shows the TEM pictures of (a) spherical-shaped PbS NPs, (b) corona formation with BSA, and (c) SAED pattern

The SAED pattern of PbS NPs confirms the single crystalline nature. PbS samples have a face center cubic structure. The diffraction planes in the SAED pattern are equivalent to the diffraction planes of the XRD pattern.

TEM pictures of cubic-shaped PbS NPs, corona formation with BSA, and SAED pattern are shown in Fig. 6.6.

The TEM picture shows the formation of BSA–cubical PbS NPs hard and soft corona.

A large number of PbS NPs with a hard corona of BSA forms a "*colony*" with 280 nm × 290 nm dimensions. The soft corona also forms in this colony. The TEM picture supports the findings which are observed from absorption kinetics. The dimension of the BSA monomer matched with the shell thickness of BSA on the core of PbS NPs confirms the attachment of BSA with PbS NPs.

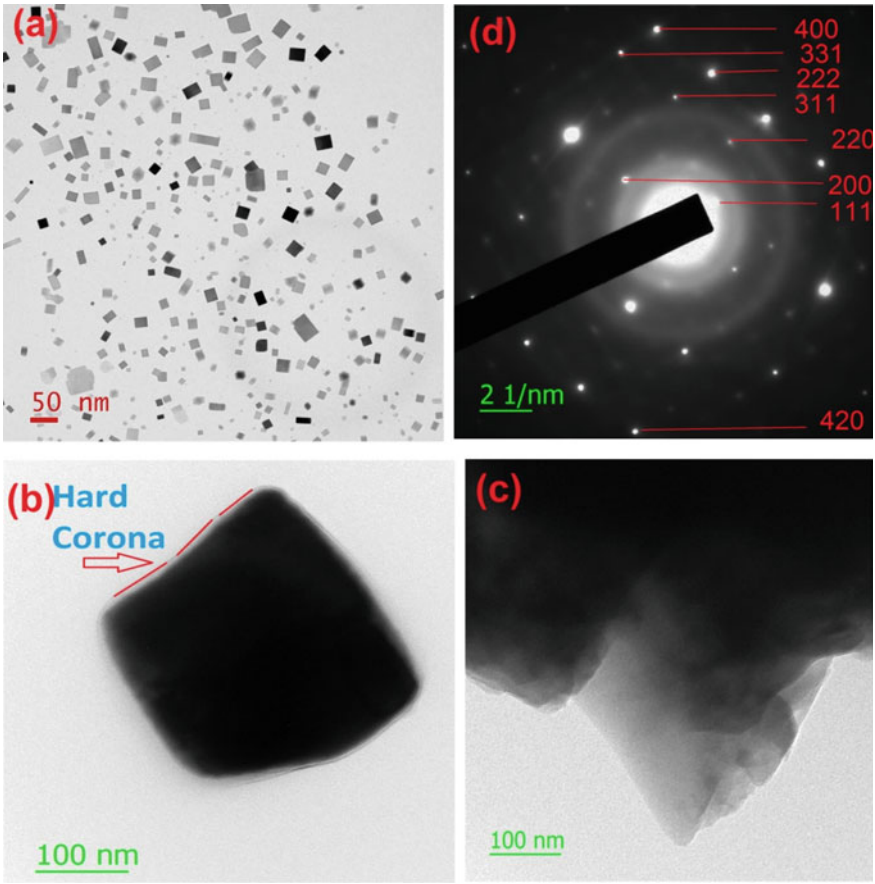

Fig. 6.6 Shows the TEM pictures of (a) cubic-shaped PbS NPs, (b, c) corona formation with BSA, and (d) SAED pattern

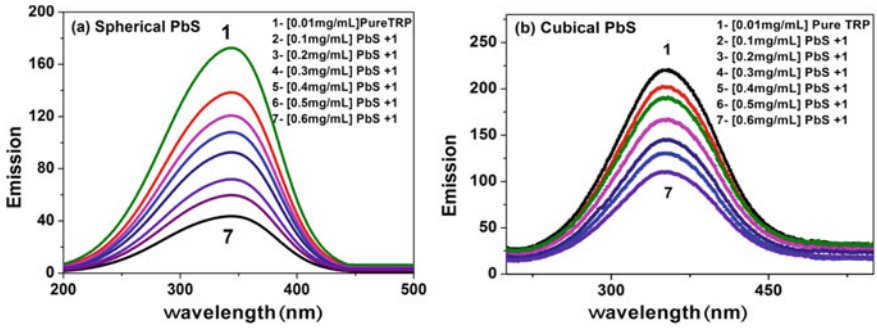

Fig. 6.7 Shows the emission spectra of tryptophan (TRY) of BSA with different concentrations of the (a) spherical PbS and (b) cubical PbS NPs

6.3.4 Emission Study

The emission spectra of TRY of BSA with different concentrations of the different shaped PbS NPs are shown in Fig. 6.7.

The PbS NPs–BSA-binding kinetics and conformational change of BSA are analyzed by fluorescence quenching measurements. The different concentrations of different shaped PbS NPs ($C_{PbS} = 0.01$–0.06 mg/mL) are added to BSA ($C_{BSA} = 0.1$ mg/mL) at room temperature and a change in the maximum intensity (I_{max}) of the fluorescence emission spectrum is observed. It is proved that the fluorescence quenching process has occurred. It also shows a maximum blue shift of about 5 nm is found with $C_{PbS} = 0.06$ mg/ml and $C_{BSA} = 0.1$ mg/mL due to hydrophobic interaction with PbS NPs. The binding of BSA with PbS NPs is analyzed by the popular Stern–Volmer equation [16].

$$\frac{F_0}{F} = K_{SV}[Q] + 1$$

F_0 and F are represented by the steady-state fluorescence intensities of fluorophore in the absence and presence of PbS NPs, respectively. K_{SV} is known as the Stern–Volmer quenching constant and [Q] represents the concentration of PbS NPs. The values of K_{SV} for different shaped PbS NPs are summarized in Table-1. The decrease of K_{SV} with increasing particle size signifies that the quenching mechanism of BSA is a dynamic quenching process in presence of PbS NPs and the strength of interaction increases with a decrease in particle size.

The plots of F_0/F versus $[Q(\mathrm{C_{PbS}})]$ and $ln\left[\frac{F_0-F}{F}\right]$ versus $ln[Q(\mathrm{CPbS}]$ for different shaped PbS NPs is shown in Fig. 6.8.

The binding constant K and the number of binding sites (n) between BSA and different shaped PbS NPs are calculated using the following equation [16]:

$$\ln\left[\frac{F_0 - F}{F}\right] = \ln K + nln[Q(CPbS)] \tag{6.1}$$

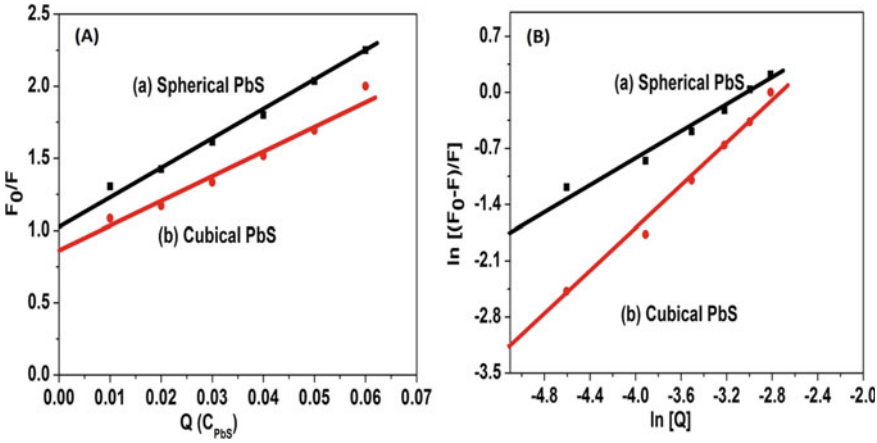

Fig. 6.8 Shows the plot of (A) F_0/F versus $Q(C_{PbS})$, and (B) $ln[\frac{F_0-F}{F}]$ versus $ln[Q(\text{CPbS}]$ for different shaped PbS NPs

Table 6.1 Comparison of parameters derived from bioconjugate analysis of BSA with PbS NPs

	K_{app}	K_{SV}	K	n
Spherical PbS NPs	7.9	19.9	23.6	1.28
Cubical PbS NPs	7.5	17.3	13.4	0.85

The plot of $ln\left[\frac{F_0-F}{F}\right]$ versus $ln[Q(C\text{PbS})]$ is a linear fit and the number of binding sites (n) is calculated from the slope of this graph.

The intercept of the straight line on the Y-axis determines the value of ln K.

The different characteristics values of bioconjugate analysis of BSA with different shaped PbS NPs are summarized in Table 6.1 and compared.

In favor of positive cooperative reaction, n > 1, reveals that once one protein molecule is bound to the NPs, its affinity for the NPs gradually increases in a super-linear fashion. However, in the case of a negative cooperative reaction, $n < 1$, the binding strength of the protein with the NPs becomes weaker as further proteins adsorb also for a non-cooperative reaction, $n = 1$ [17–22]. In the case of cubic PbS NPs, the negative cooperative reaction with BSA is found. However, for spherical PbS NPs, a positive cooperative reaction with BSA is found. Therefore, the affinity of BSA to the PbS NPs gradually increases in a superlinear fashion, which also supports the observation obtained from HRTEM images.

The interaction PbS NPs with TRY is studied to investigate the probable binding sites of BSA with PbS NPs. The value of n in case of interaction of PbS NPs with TRY for spherical PbS NPs almost matched with the PbS NPs–BSA complex. Therefore, TRY are the probable binding sites of BSA with PbS NPs as well as its affinity to PbS NPs increases with the decrease of NP size.

6.4 Conclusion

Simple chemically synthesized PbS NPs show the lowest energy excitonic band edge transition and emission in the NIR region. This formation of "*hard*" and "*soft*" corona is studied by the UV–VIS–NIR absorption along with TEM. The exponential association mechanism is followed for "PbS NPs-BSA" corona formation and corona formation starts immediately after incorporation of PbS NPs into BSA as well as the unfolding of BSA continues for a very long time. The enlarged image of a hard corona represents that the core PbS NPs are fully covered with BSA with a shell thickness of 7.5 nm, matched with a dimension of BSA (~8 nm). A large number of PbS NPs with a hard corona of BSA forms a " *colony*" with diameters in the range of 260 nm. The "*soft corona*" also grows on this colony. The fluorescence study reveals that the quenching of fluorescence BSA in presence of PbS NPs follows the dynamic quenching process and TRY is the major binding site. Nearest to spherical PbS NPs, the positive cooperative reaction between PbS NPs and BSA is found and the affinity of BSA to the PbS NPs gradually increases in a superlinear fashion.

Acknowledgements The authors would like to acknowledge the DST-FIST-sponsored Department of Physics, Vidyasagar University, for providing various instrumental facilities.

References

1. O. Khullar, J.V. Frangioni, M. Grinstaff, Y.L. Colson, Image-guided sentinel lymph node mapping and nanotechnology-based nodal treatment in lung cancer using invisible near-infrared fluorescence light. Thorac. Cardioid Surg. **21**, 309–315 (2009)
2. S. Cohen, S. Margel, Engineering of near IR fluorescent albumin nanoparticles for in vivo detection of colon cancer. J. Nanobiotechnology **10**, 36 (2012)
3. R.K. Joshi, H.K. Sehgal, Density of states near Fermi level in PbS nanoparticle films. Phys. E. **23**, 168–170 (2004)
4. E. Hellstrand, I. Lynch, A. Andersson, T. Drakenberg, B. Dahlbäck, K.A. Dawson, S. Linse, T. Cedervall, Complete high-density lipoproteins in nanoparticle corona. FEBS J. **276**, 3372 (2009)
5. S. Milani, F. Baldelli Bombelli, A. S. Pitek, K. A. Dawson, and J. Rädler, Reversible versus irreversible binding of transferrin to polystyrene nanoparticles: soft and hard corona. ACS Nano **6**, 2532 (2012).
6. E. Casals, T. Pfaller, A. Duschl, G.J. Oostingh, and V. Puntes, Time evolution of the nanoparticle protein corona. ACS Nano **4**, 3623 (2010).
7. J. Klein, Surface interactions with adsorbed macromolecules. J. Colloid Interface Sci. **111**, 305–313 (1986)
8. S.R. Saptarshi, A. Duschl, A.L. Lopata, Interaction of nanoparticles with proteins: relation to bio-reactisvity of the nanoparticle. J. Nanobiotechnol. **11**, 26 (2013)
9. T. Cedervall, I. Lynch, M. Foy, T. Berggård, S.C. Donnelly, G. Cagney, S. Linse, and K.A. Dawson, Effect of membrane charge density on the protein corona of cationic liposomes: interplay between cationic charge and surface area. Angew. Chem. Int.Ed. **119**, 5856 (2007).
10. D. Dell'Orco, M. Lundqvist, C. Oslakovic, T. Cedervall, and S. Linse, Modeling the time evolution of the nanoparticle-protein corona in a body fluid. PLoS One. **5**, e10949 (2010).

11. I. Lynch, T. Cedervall, M. Lundqvist, C. Cabaleiro-Lago, S. Linse, and K.A. Dawson, The nanoparticle-protein complex as a biological entity; a complex fluid and surface science challenge for the 21st century. Adv. Colloid Interface Sci. **167**, 134 (2007).
12. I. Lynch, K.A. Dawson, Protein-nanoparticle interactions. Nano Today **3**, 40 (2008)
13. I. Lynch, K.A. Dawson, and S. Linse, Detecting cryptic epitopes created by nanoparticles. Sci. Signal **327**, pe14 (2006).
14. F. Ding, S. Radic, R. Chen, P. Chen, N.K. Geitner, J.M. Brown, P.C. Ke, Direct observation of a single nanoparticle–ubiquitin corona formation. Nanoscale **5**, 9162 (2013)
15. H. Yin, R. Chen, P. Casey, P. Ke, T. Davis, C. Chen, Reducing the cytotoxicity of ZnO nanoparticles by a pre-formed protein corona in a supplemented cell culture medium. RSC Adv. **5**, 73963 (2015)
16. S. Dominguez-Medina, L. Kisley, L.J. Tauzin, A. Hoggard, B. Shuang, A.S.D.S. Indrasekara, S. Chen, L.Y. Wang, P.J. Derry, A. Liopo, Adsorption and unfolding of a single protein triggers nanoparticle aggregation. ACS Nano **10**, 2103 (2016)
17. C. Vidaurre-Agut, E. Rivero-Buceta, E. Romaní-Cubells, A.M. Clemments, C.D. Vera-, C.C. Landry, P. Botella, Protein corona over mesoporous silica nanoparticles: influence of the pore diameter on competitive adsorption and application to prostate cancer diagnostics. ACS Omega **4**(5), 8852–8861 (2019)
18. S. Dominguez-Medina, J. Blankenburg, J. Olson, C.F. Landes, S. Link, Adsorption of a protein monolayer via hydrophobic interactions prevents nanoparticle aggregation under harsh environmental conditions. ACS Sustain. Chem. Eng. **1**, 833 (2013)
19. P. Wang, X. Wang, L. Wang, X. Hou, W. Liu, and C. Chen, *In vitro* biomechanical properties, fluorescence imaging, surface-enhanced Raman spectroscopy, and photothermal therapy evaluation of luminescent functionalized $CaMoO_4$:Eu@Au hybrid nanorods on human lung adenocarcinoma epithelial cells. Sci. Technol. Adv. Mater. **16**, 034610 (2016).
20. W. Liu, J. Rose, S. Plantevin, M. Auffan, J.Y. Bottero, C. Vidaud, Protein corona formation for nanomaterials and proteins of a similar size: hard or soft corona. Nanoscale **5**, 1658 (2013)
21. R. Huang, R.P. Carney, K. Ikuma, F. Stellacci, B.L. Lau, Effects of surface compositional and structural heterogeneity on nanoparticle-protein interactions: different protein configurations. ACS Nano **8**, 5402 (2014)
22. W. Zhou, Y. Cao, D. Sui, W. Guan, C. Lu, J. Xie, Ultrastable BSA-capped gold nanoclusters with a polymer-like shielding layer against reactive oxygen species in living cells. Nanoscale **8**, 9614 (2016)
23. A.K. Mishra, A.K. Bhunia, S. Saha, Lead sulfide quantum dot–serum albumin bioconjugate: spectroscopic, microscopic investigation and photo-conducting current analysis. Appl. Phys. A **127**, 316 (2021)
24. A.K. Mishra, S. Saha, Photocatalytic activity of methylene blue in the presence of PbS nanoparticles and its comparison with bulk PbS. Int. J. Metall. & Mater. Sci. Eng. **10**(1), 13–20 (2020)
25. C. Louis-June, M.A. Andrade-Navarro, C. Perez-, Prediction of protein secondary structure from circular dichroism using theoretically derived spectra. Protein **80**, 374 (2012)
26. O.K. Abou-Zied, O.I. Al-, Characterization of subdomain IIA binding site of human serum albumin in its native, unfolded, and refolded states using small molecular probes. J. Am. Chem. Soc. **130**, 10793 (2008)
27. T. Chakraborty, I. Chakraborty, S.P. Moulik, S. Ghosh, Physicochemical and conformational studies on BSA-surfactant interaction in aqueous medium. Langmuir **25**, 3062 (2009)
28. I.R. Krauss, F. Sica, C.A. Mattia, A. Merlino, Physicochemical and conformational studies on BSA-surfactant interaction in aqueous medium. Int. J. Mol. Sci. **13**, 3782 (2012)
29. M. Carbonaro, P. Maselli, P. Dore, A. Nucara, Pulse foods: Processing, quality and nutraceutical applications. Food Chem. **108**, 361 (2008)
30. A.K. Mishra, S. Saha, Comparison of ethanol gas sensors based on PbS nanoparticles and bulk PbS. Int. J. Electrochem. Sci. **15**, 11594–11605 (2020)
31. A.K. Mishra, S. Saha, Growth and characterization of PbS nanoparticles using THF. J. Phys. Sci. **23**, 223–229 (2018)